Supplementary Material: *A Quantitative Characterization of the Spatial Distribution of Brain Metastases from Breast Cancer and Respective Molecular Subtypes*

Saeedeh Mahmoodifar, M.S.,[3] Dhiraj J. Pangal, B.S.,[1] Tyler Cardinal, B.S.,[1] David Craig, Ph.D.,[4] Thomas Simon, Ph.D.,[4] Ben Yi Tew, Ph.D.,[4] Wensha Yang, Ph.D.,[6] Eric Chang, M.D.,[6] Min Yu, Ph.D.,[6] Josh Neman, Ph.D.,[1] Jeremy Mason, Ph.D.,[5] Arthur Toga, Ph.D.,[6] Bodour Salhia, Ph.D.,[4] Gabriel Zada, M.D., M.S.,[1] and Paul K. Newton, Ph.D.[2,*]

[1]*Department of Neurosurgery Keck School of Medicine of University of Southern California 1300 N. State Street, Suite 3300 Los Angeles, CA 90033*

[2]*Department of Aerospace and Mechanical Engineering, Mathematics and The Ellison Institute for Transformative Medicine of University of Southern California*
Viterbi School of Engineering of University of Southern California 854 Downey Way Los Angeles, CA 90089

[3]*Department of Physics Astronomy of University of Southern California Los Angeles, CA 90089*

[4]*Department of Translational Genomics Keck School of Medicine of University of Southern California 1450 Biggy Street Los Angeles, CA 90033*

[5]*Convergent Science Institute in Cancer, Michelson Center for Convergent Bioscience of University of Southern California, Los Angeles, CA 90089*
Catherine Joseph Aresty Department of Urology, Institute of Urology, Keck School of Medicine of University of Southern California, Los Angeles, CA 90033

[6]*Keck School of Medicine of University of Southern California, Los Angeles, CA 90033*

[*]*newton@usc.edu*

Disclosure: The authors have no conflicts of interest to disclose.

Abstract

Purpose: Brain metastases (BM) remain a significant cause of morbidity and mortality in breast cancer (BC) patients. Specific factors promoting the process of BM and predilection for selected neuro-anatomical regions remain unknown, yet may have major implications for prevention or treatment. Anatomical spatial distributions of BM from BC suggest a predominance of metastases in the hindbrain and cerebellum. Systematic approaches to quantifying BM location or location-based analyses based on molecular subtypes, however, remain largely unavailable.
Methods: We analyzed stereotactic Cartesian coordinates derived from 134 patients undergoing gamma- knife radiosurgery (GKRS) for treatment of 407 breast cancer BMs to quantitatively study BM spatial distribution along principal component axes and by intrinsic molecular subtype (ER,PR,Herceptin). We used kernal density estimators (KDE) to highlight clustering and distribution regions in the brain, and we used the metric of mutual information (MI) to tease out subtle differences in the BM distributions associated with different molecular subtypes of BC. BM location maps according to vascular and anatomical distributions using Cartesian coordinates to aid in systematic classification of tumor locations were additionally developed.
Results: We corroborated that BC BMs show a consistent propensity to arise posteriorly and caudally, and that Her2+ tumors are relatively more likely to arise medially rather than laterally. To compare the distributions among varying BC molecular subtypes, the mutual information metric reveal that the ER-PR-Her2+ and ER-PR-Her2- subtypes show the smallest amount of mutual information and are most molecularly distinct. The kernel density contour plots show a propensity for triple negative BC to arise in more superiorly or cranially situated BMs.
Conclusions: We present a novel and shareable workflow for characterizing and comparing

spatial distributions of BM which may aid in identifying therapeutic or diagnostic targets and interactions with the tumor microenvironment. Further characterization of these patterns with larger multi-institutional data-sets may have major impacts on treatment or management of cancer patients.

Supplementary Material

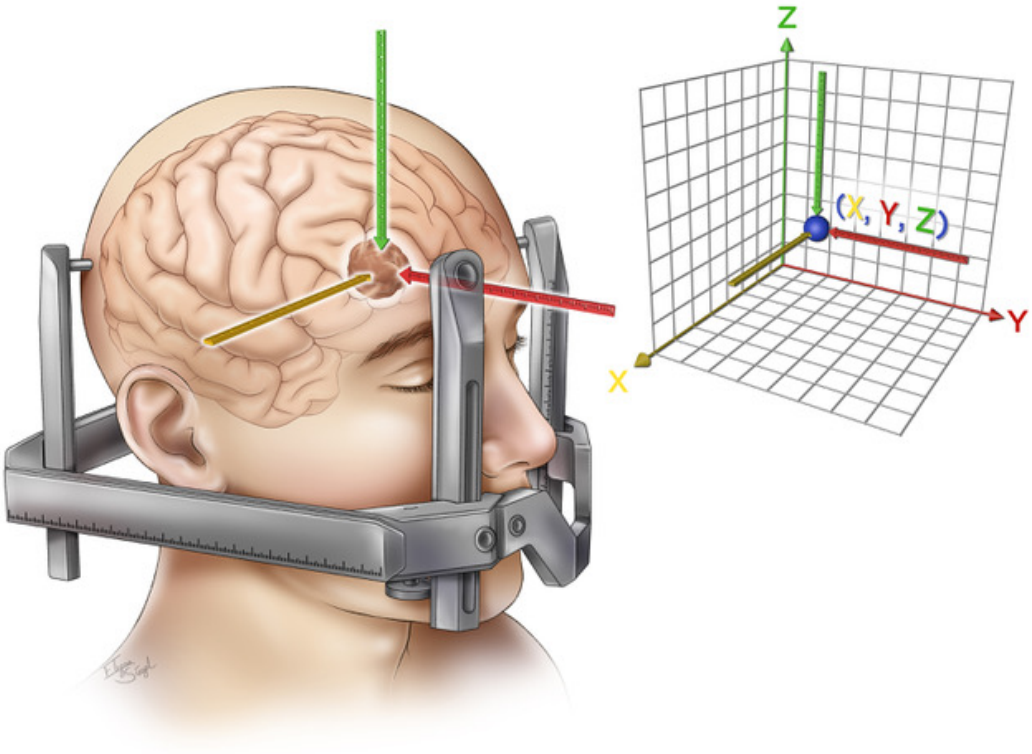

Fig. S1. Schematic illustration of Gamma Knife radiosurgery (GKRS) stereotactic headset, intracranial metastasis (brown), and targeted radiation location in X (yellow), Y (Red) and Z (Green) planes. These coordinates are subsequently mapped to a traditional three dimensional cartesian plane (right), and repeated for all brain metastases for all patients undergoing GKRS at our institution.

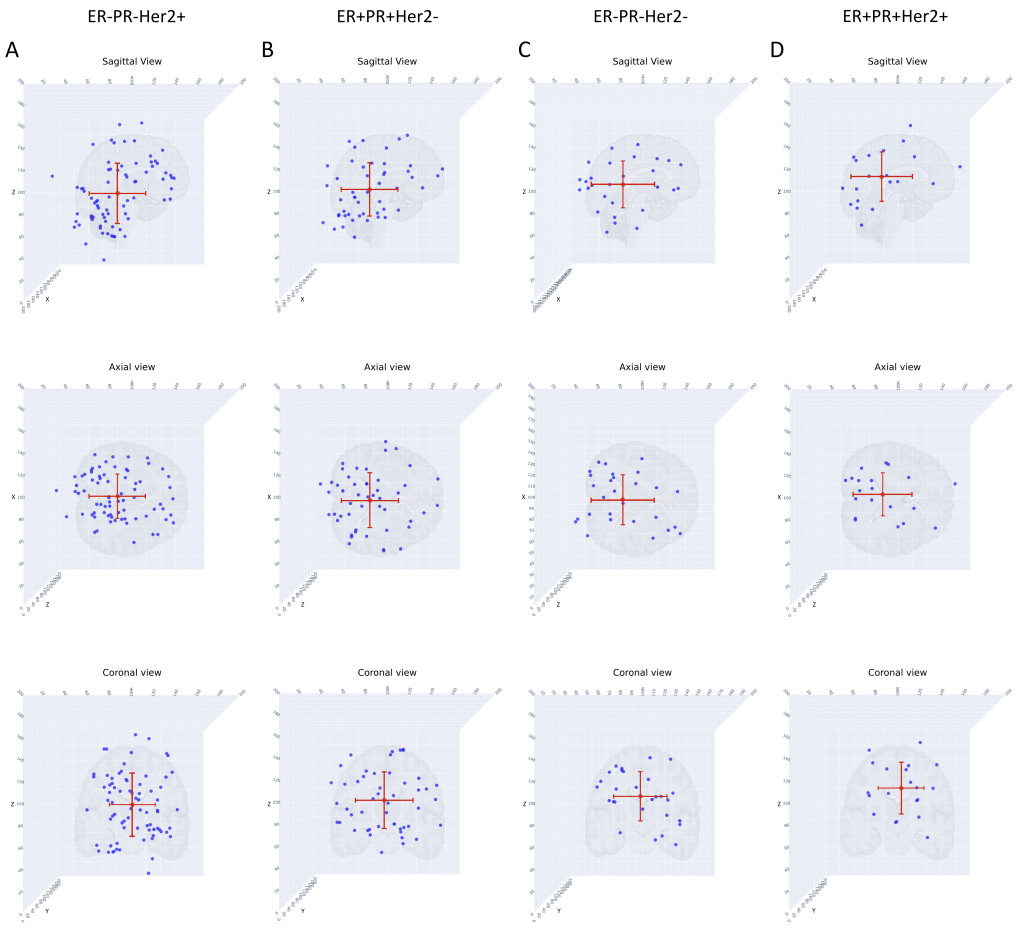

Fig. S2. Scatter plots of metastatic tumor distributions according to genetic subgroups, sagittal, axial, and coronal views. Red dot indicates mean. A) Column showing ER-/PR-/Her2+ subgroup, three views; B) Column showing ER+/PR+/Her2- subgroup, three views; C) Column showing TNBC subgroup, three views; D) Column showing TPBC subgroup, three views.

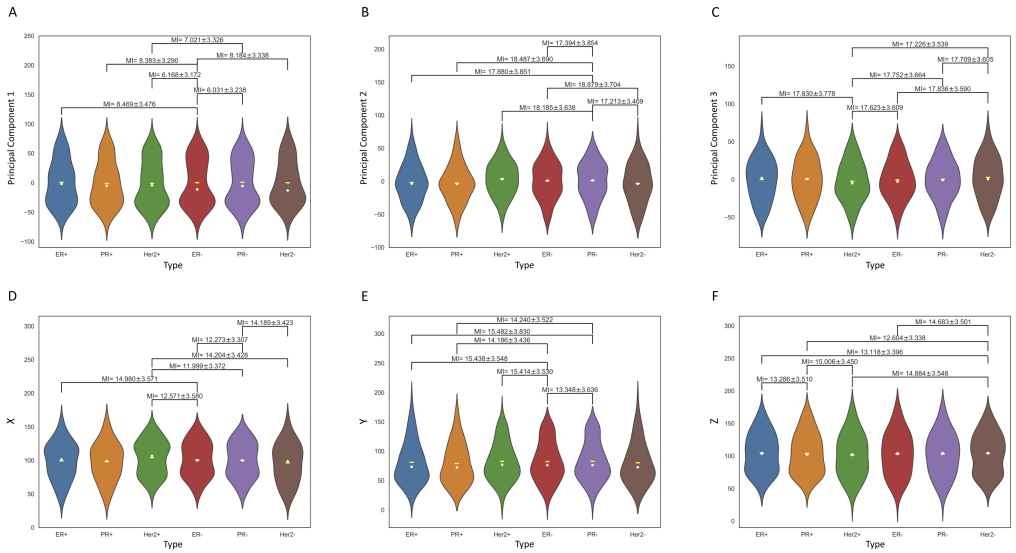

Fig. S3. Violin plots (probability distribution functions) of metastatic distributions according to molecular subtype (indicated by color), comparing distributions in original Cartesian X-Y-Z coordinates, and Principal component coordinates (PC1-PC2-PC3). MI metric is shown for each pair. A) Distribution along PC1-axis according to molecular subtype. Yellow dash indicates mean, white dot indicates median; B) Distribution along PC2-axis according to subtype. Yellow dash indicates mean, white dot indicates median; C) Distribution along PC3-axis according to subtype. Yellow dash indicates mean, white dot indicates median; D) Distribution along X-axis according to molecular subtype. Yellow dash indicates mean, white dot indicates median. We use this representation to arrange the subtypes from left to right in order of increasing divergence between the means and medians; E) Distribution along Y-axis according to molecular subtype. Yellow dash indicates mean, white dot indicates median; F) Distribution along Z-axis according to molecular subtype. Yellow dash indicates mean, white dot indicates median.

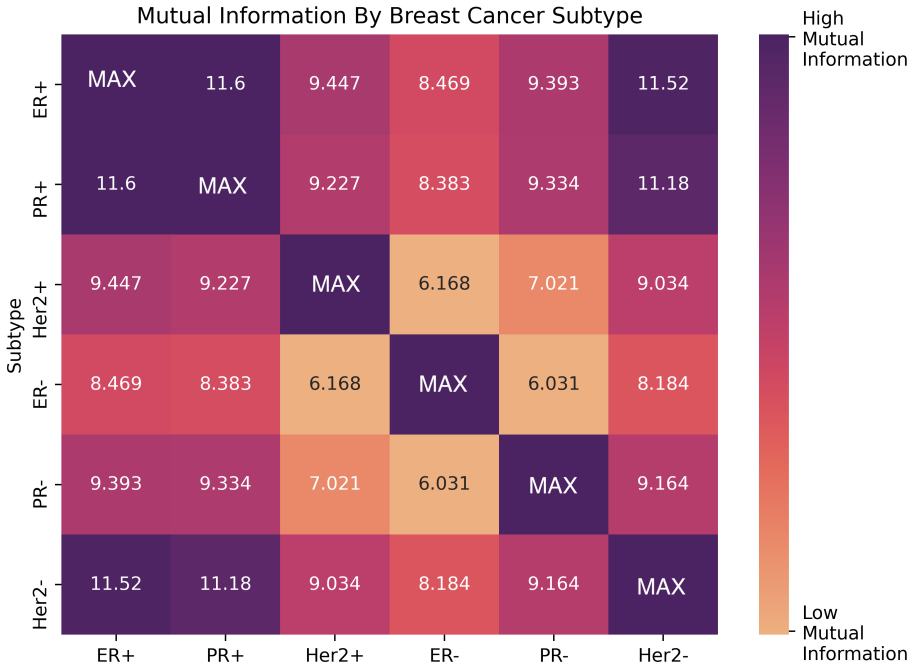

Fig. S4. Mutual information heat map for the six breast cancer molecular subtypes along PC1-axis. Low mutual information indicates the distributions associated with the two subtypes are not highly dependent. High mutual information indicates the distributions associated with the two subtypes are highly dependent.

ER	PR	Her2/Neu	No. Metastases	Anterior : Posterior : Watershed	Lateral : Medial	Median X Axis	Median Y Axis	Median Z Axis	Median PC1 Axis	Median PC2 Axis	Median PC3 Axis
+			110	28:42:40	25:85	101.35	73.30	103.85	-3.13	0.12	2.98
-			116	31:56:29	21:95	99.90	76.30	103.60	-10.56	-1.05	2.80
	+		86	19:35:32	21:65	98.85	72.15	102.45	-3.42	-0.35	1.02
	-		124	32:57:35	23:101	99.90	76.30	103.85	-4.93	-1.13	1.64
		+	124	27:60:37	22:102	106.80	76.80	101.80	-2.56	-0.77	1.74
		-	91	23:37:31	25:66	98.70	72.70	104.20	-9.31	0.55	-0.33
+	+	+	20	4:8:8	3:17	110.25	69.35	114.30	-2.91	-1.08	-7.26
+	+	-	49	10:20:19	16:33	100.4	73.90	99.1	-3.98	1.19	-2.01
-	-	+	75	17:40:18	12:63	99.60	77.90	93.90	-9.56	0.28	2.25
-	-	-	28	8:11:9	7:21	103.45	66.20	107.15	-12.98	-0.58	-1.04
+	-	+	8								
-	+	+	4								
+	-	-	5								
-	+	-	2								

Table S1. Number of brain metastases and proportion of different spatial subgroupings along with the medians in Cartesian and Principal Component coordinates by tumor subtype. The last four molecular subgroupings (last four rows) are not considered in this paper due to the small number of data points.

	PC1	PC2	PC3	X	Y	Z
ER-PR-Her2+/ ER-PR-Her2-	8.966 ± 3.394	15.508 ± 3.330	16.350 ± 3.655	13.023 ± 3.466	15.548 ± 3.648	16.878 ± 3.600
ER+PR+Her2-/ ER-PR-Her2+	10.767 ± 3.443	17.467 ± 3.496	18.515 ± 3.801	15.805 ± 3.457	17.472 ± 3.694	15.132 ± 3.532
ER+PR+Her2+ / ER-PR-Her2+	10.979 ± 3.376	17.392 ± 3.667	21.222 ± 3.881	14.446 ± 3.645	17.146 ± 3.745	18.476 ± 3.658
ER+PR+Her2-/ ER-PR-Her2-	12.540 ± 3.527	15.359 ± 3.531	16.221 ± 3.548	14.470 ± 3.536	16.200 ± 3.607	14.571 ± 3.503
ER+PR+Her2+/ ER-PR-Her2-	12.614 ± 3.376	15.249 ± 3.606	18.921 ± 3.789	13.100 ± 3.613	16.029 ± 3.504	18.112 ± 3.677
ER+PR+Her2+ / ER+PR+Her2-	14.808 ± 3.589	17.018 ± 3.530	20.996 ± 3.820	16.014 ± 3.547	18.158 ± 3.645	16.247 ± 3.766
PR- / ER-	6.031 ± 3.238	17.394 ± 3.854	17.993 ± 3.653	12.273 ± 3.307	13.348 ± 3.636	17.442 ± 3.644
Her2+ / ER-	6.168 ± 3.172	19.844 ± 3.765	17.623 ± 3.609	12.571 ± 3.580	15.414 ± 3.530	17.102 ± 3.598
Her2+ / PR-	7.021 ± 3.326	18.185 ± 3.638	17.752 ± 3.664	11.999 ± 3.372	15.715 ± 3.678	17.683 ± 3.720
Her2- / ER-	8.184 ± 3.338	18.879 ± 3.704	17.836 ± 3.590	14.506 ± 3.569	16.038 ± 3.762	14.683 ± 3.501
PR+ / ER-	8.383 ± 3.290	20.139 ± 3.885	18.164 ± 3.536	15.609 ± 3.565	14.186 ± 3.436	15.196 ± 3.607
ER+ / ER-	8.469 ± 3.476	19.238 ± 3.652	17.926 ± 3.622	15.484 ± 3.515	15.438 ± 3.548	15.482 ± 3.679
Her2+ / Her2-	9.034 ± 3.363	19.914 ± 3.792	17.226 ± 3.539	14.204 ± 3.428	18.322 ± 3.758	14.884 ± 3.548
PR- / Her2-	9.164 ± 3.319	17.213 ± 3.469	17.709 ± 3.605	14.189 ± 3.423	15.927 ± 3.691	15.359 ± 3.520
Her2+ / PR+	9.227 ± 3.452	21.094 ± 3.730	18.118 ± 3.514	15.350 ± 3.506	16.584 ± 3.661	15.006 ± 3.450
PR+ / PR-	9.334 ± 3.323	18.487 ± 3.690	18.253 ± 3.550	15.325 ± 3.542	14.24 ± 3.522	15.662 ± 3.541
ER+ / PR-	9.393 ± 3.582	17.88 ± 3.851	18.09 ± 3.490	14.980 ± 3.571	15.482 ± 3.830	16.098 ± 3.715
Her2+ / ER+	9.447 ± 3.351	20.288 ± 3.861	17.830 ± 3.778	15.093 ± 3.558	17.836 ± 3.753	15.588 ± 3.586
PR+ / Her2-	11.178 ± 3.466	20.357 ± 3.804	17.978 ± 3.604	17.838 ± 3.564	16.798 ± 3.715	12.604 ± 3.338
ER+ / Her2-	11.516 ± 3.469	19.579 ± 3.714	17.827 ± 3.669	17.216 ± 3.831	18.183 ± 3.745	13.118 ± 3.396
ER+ / PR+	11.601 ± 3.455	20.712 ± 3.723	18.224 ± 3.532	18.455 ± 3.691	16.696 ± 3.625	13.286 ± 3.510

Table S2. Mutual Information. Ranked listing (from smallest to largest) of MI between pairs of molecular subtypes along each of the coordinate axes, using the PC1 coordinate axis values to order the list. Smaller MI values indicate weaker mutual dependence (i.e. more independence), larger MI values indicate stronger mutual dependence.